

Article

Optimization of Magnetic Gear Patterns Based on Taguchi Method Combined with Genetic Algorithm

Yuan Mao ¹ and Yun Yang ^{2,*}

¹ College of Information Engineering, Zhejiang University of Technology, Hangzhou 310023, China; maoyuan@zjut.edu.cn

² Department of Electrical Engineering, The Hong Kong Polytechnic University, Hong Kong, China

* Correspondence: yunyang@polyu.edu.hk; Tel.: +852-2766-6186

Abstract: Magnetic gears (MGs) have gained increasing attention due to their sound performance in high torque density and low friction loss. Aiming to maximize the torque density, topology design has been a popular issue in recent years. However, studies on the optimization comparisons of a general MG topology pattern are very limited. This paper proposes a Taguchi-method-based optimization method for a general MG topology pattern, which can cover most of the common types of radially magnetized concentric-surface-mounted MGs (RMCSM-MGs). The Taguchi method is introduced to evaluate the influence of each parameter in MGs. Moreover, the parameter value range is re-examined based on the sensitivity analysis results. The genetic algorithm (GA) method is adopted to optimize the topology pattern in the study.

Keywords: finite element method; genetic algorithm; magnetic gear; Taguchi method



Citation: Mao, Y.; Yang, Y. Optimization of Magnetic Gear Patterns Based on Taguchi Method Combined with Genetic Algorithm. *Energies* **2022**, *15*, 4963. <https://doi.org/10.3390/en15144963>

Academic Editor: Andrea Mariscotti

Received: 23 May 2022

Accepted: 21 June 2022

Published: 6 July 2022

Publisher's Note: MDPI stays neutral with regard to jurisdictional claims in published maps and institutional affiliations.



Copyright: © 2022 by the authors. Licensee MDPI, Basel, Switzerland. This article is an open access article distributed under the terms and conditions of the Creative Commons Attribution (CC BY) license (<https://creativecommons.org/licenses/by/4.0/>).

1. Introduction

Wind power generation has become more and more popular in industrial production and daily life due to its clean and inexhaustible advantages over traditional coal-fired power [1]. Gearboxes are widely used in wind power generation systems. Components of different speeds can be made to run at certain speed ratios by connecting them through gearboxes. Mechanical gears, which are currently widely used in industry, suffer from the following problems: loud noise, high manufacturing and installation accuracy requirements, high friction loss, etc., [2]. In recent years, due to the development of rare earth materials, magnetic gears (MGs) are expected to replace mechanical gears [3]. Abundant research and experiments have indicated that the transmission torque of MGs can reach up to 100 kNm/m³ [4]. In addition, MGs have the advantages of physical isolation, lower maintenance costs, and inherent overload protection [5].

The main material required for MGs is rare-earth permanent magnets (PMs), which are expensive. Hence, there is an increasing concern regarding saving PM material without sacrificing the torque density. There have been several longitudinal studies involving optimizing the MG topology to save resources and costs. To meet application requirements, studies on the topology design of radially magnetized concentric-surface-mounted MGs (RMCSM-MGs) have become popular in recent years. It is well-known that RMCSM-MGs are commonly made of three layers. Traditional RMCSM-MGs have PMs embedded in the inner layer and outer layer, while the middle layer is made of ferrite material. Another kind of MG with competitive performance is the triple-PM-excited MGs, which have PMs embedded in each layer. The torque per unit PM volume among the six basic topologies of triple-PM-excited MGs is compared in [6]. However, the six types of topologies have the same outer rotor structure and modulation ring structure. Only the topology of the inner rotor is changed during the comparison. In [7], the author attempted to propose a pattern design for the triple-PM-excited MGs. However, the unipolar permanent magnetic-ferrite array and the air-ferrite array of the inner rotor and modulation ring are not considered in

this pattern. Moreover, optimization of the PM and ferrite distribution is mostly ignored in the literature; the assumption that PM and ferrite are equally distributed is taken by default, without any explanation.

Research on this subject has been mostly restricted to individually optimizing each type of MG, which may cost an amount of time. This paper aims to optimize and comprehensively compare the topology of common RMCSM-MGs. Therefore, a topology pattern was designed, which could cover most of the common types of RMCSM-MGs. In previous studies, authors often needed to optimize once for each MG structure [8–10]. By resorting to pattern design, optimization must be performed only once [11,12]. The optimization method used in this article is the genetic algorithm (GA). Local convergence, the so-called “premature phenomenon”, is a problem that has always plagued researchers. Common solutions include increasing the probability of mutation, increasing diversity, and reducing the probability of selecting excellent chromosomes [13]. However, these approaches may result in a higher amount of computation. In this paper, the Taguchi method is employed to obtain a near-optimal value, which can help to determine the appropriate initial values and ranges in GA optimization [14–16]. The Taguchi method has been widely used in the field of industrial engineering. To name a few applications, the parameters of the Jiles–Atherton hysteresis model are optimized using Taguchi’s method in [17], and the author of [18] blended the Taguchi orthogonal array (OA) concept into the design of the linear antenna array. In [19], the Taguchi method is employed to optimize the material of multiple layers of dielectric thin films in the photonic radiative cooler. Many other applications of the Taguchi method were reviewed in [20–22], among other studies.

2. General Pattern Design

The RMCSM-MG is mainly composed of three rings. The inner and the outer ring can rotate, so they are named rotors. The middle ring is stationary, and is named the modulation ring. It is worth noting that the PMs of the RMCSM-MG are magnetized in radial directions. As shown in Figure 1, the rotors may be designed as a bipolar PM array, unipolar PM array, or bipolar PM–ferrite array [23]. As presented in Figure 2, the modulation ring may be created as a ferrite–air array, ferrite–PM array, or ferrite–PM–air array [23]. Hence, there are 27 possible topologies of RMGSM-MG, which are discussed in this study. The intuitive approach is to separately optimize each of the 27 types, but this requires a lot of computation. In this article, we design a pattern to cover these 27 special structural types. This can greatly reduce the amount of computation.

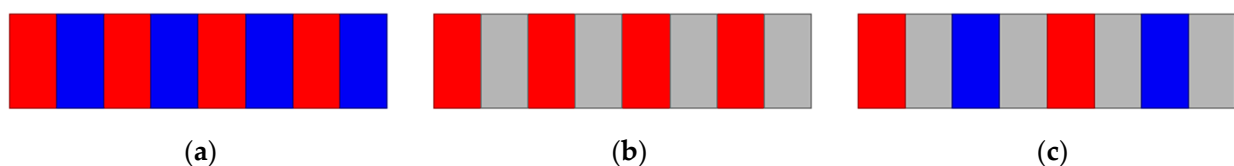


Figure 1. Three kinds of rotor arrays: (a) bipolar PM array (b) unipolar PM array (c) bipolar PM–ferrite array [23].

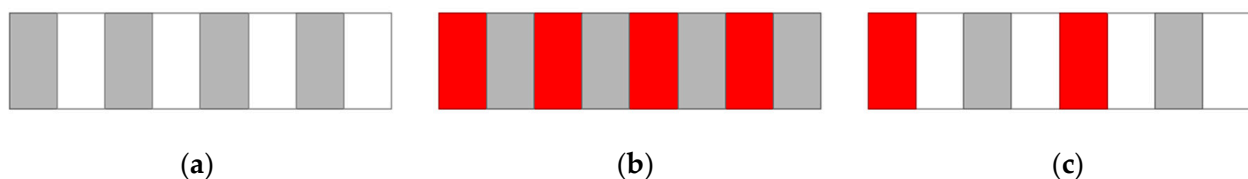


Figure 2. Three kinds of modulation arrays: (a) ferrite–air array (b) ferrite–PM array (c) ferrite–PM–air array [23].

The configuration of the RMCSM-MG pattern is shown in Figure 3. It is well-known that the working principle of MGs obeys the modulation effect [24], and the proposed RMGSM-MG pattern in this article is no exception. Figure 4 is a partially enlarged drawing

of the RMGSM-MG pattern in Figure 3. The red and blue segments represent the S and N pole PMs made from NdFeB material, respectively. The magnetization directions are marked in the figure. The grey segments are ferrite pieces made of M19_24G material. The flux path of both inner and outer rotor PM poles before modulation is shown. After modulation, the inner rotor flux path has the same pole pair number as that of the outer rotor. Similarly, the outer rotor can be modulated to match the PM pole pair of the inner rotor. Thus, they can transmit torque steadily between each rotor at any different rotational speed. For this reason, the pole pair number of each layer can be summarized by the following equations:

$$p_o = |p_i - m| \quad \text{or} \quad p_i = |p_o - m| \tag{1}$$

where p_i and p_o represent the inner and outer pole pair numbers, respectively. The quantity m represents the segment of modulation ferrite.

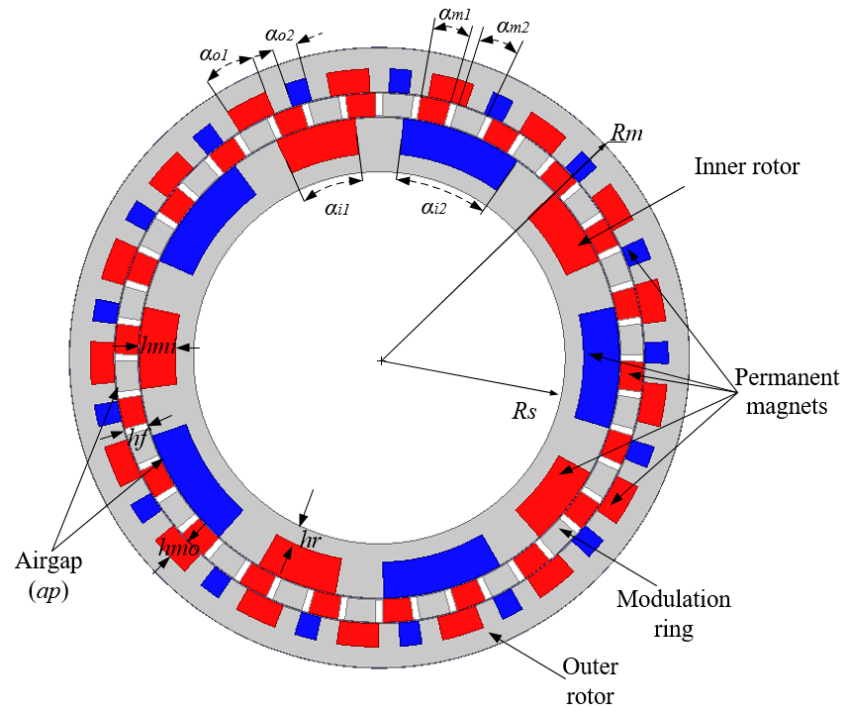


Figure 3. Configuration of RMCSM-MG pattern.

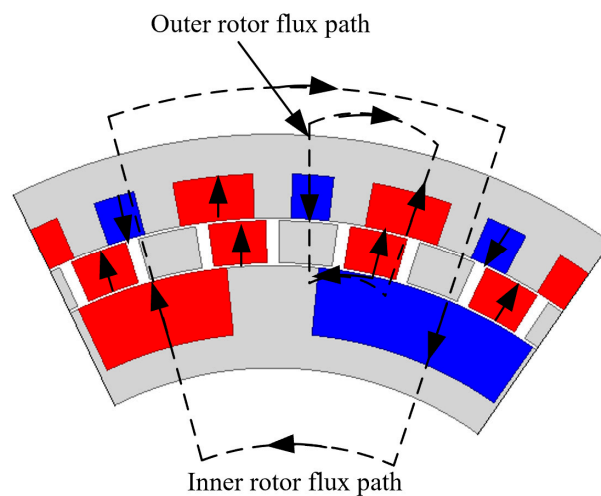


Figure 4. Flux path of inner and outer rotor PM poles before modulation.

The parameters of the RMCSM-MG pattern are shown in Table 1. As shown in Figure 3, the innermost radius, $R_s = 60$ mm, and the outermost radius, $R_m = 105$ mm, are also constant to keep the total volume of the MG invariable. For each layer, the distribution of PM and ferrite segments is re-examined by setting the expansion angles as variables. It can be deduced that the PM and ferrite arrays shown in Figures 1 and 2 are particular cases included in the general pattern. For instance, Figure 1a shows the rotor arrays when $\alpha_{i1} = \alpha_{i2}$ or $\alpha_{o1} = \alpha_{o2}$. Figure 1b shows the case when $\alpha_{i1} = 180^\circ/p_i$, $\alpha_{i2} = 0$ or $\alpha_{o1} = 180^\circ/p_o$, $\alpha_{o2} = 0$.

Table 1. Main parameters of the pattern of RMCSM-MG.

Symbol	Meaning	Value
p_i	inner rotor pole pair number	5
p_o	outer rotor pole pair number	17
m	modulation ferrite segments	22
ag	airgap length	0.5 mm
lg	axial length	65 mm
h_{mi}	inner layer height	variable
h_f	middle layer height	variable
h_{mo}	outer layer height	variable
h_r	inner rotor height	variable
R_s	innermost radius	60 mm
R_m	outermost radius	105 mm
α_{i1}	angle of inner layer S pole	variable
α_{i2}	angle of inner layer N pole	variable
α_{m1}	angle of middle layer S pole	variable
α_{m2}	angle of middle layer ferrite pole	variable
α_{o1}	angle of outer layer S pole	variable
α_{o2}	angle of outer layer N pole	variable
μ_r	relative permeability	1.044
H_c	magnetic coercivity	-8.38×10^5 A/m

3. Sensitivity Analysis and Optimization

By employing a Taguchi-method-based sensitivity analysis, it is possible to discover a near-optimal solution. In this study, the value range in the optimization is refined according to the near-optimal solution. It is well-known that each parameter will be given an upper boundary and lower boundary in a random search optimization algorithm [25–27]. In the Taguchi method, each parameter is evaluated on several specific levels [18].

Parameters to be optimized are listed in Table 1. Assume \mathbf{X} represents the array of parameters, and $C(\mathbf{X})$ represents the torque per unit PM volume, which can be expressed as follows:

$$C(\mathbf{X}) = T(\mathbf{X})/V_{PM}(\mathbf{X}) \quad (2)$$

where $T(\mathbf{X})$ is the average electromagnetic torque of the inner rotor and outer rotor in one rotation period, and $V_{PM}(\mathbf{X})$ is the total volume of the PM pieces. The optimization criterion of this study is to maximize $C(\mathbf{X})$. It is worth noting that the unit of $C(\mathbf{X})$ is kNm/m^3 .

Some linear constraints are also added to ensure that the geometry is logical:

$$\left\{ \begin{array}{l} \alpha_{i1} + \alpha_{i2} \leq \frac{360^\circ}{p_i} \\ \alpha_{m1} + \alpha_{m2} \leq \frac{360^\circ}{n_s} \\ \alpha_{o1} + \alpha_{o2} \leq \frac{360^\circ}{p_o} \\ hf + h_{mi} + h_{mo} + h_r < R_m - R_s - 2 \cdot ap \end{array} \right. \quad (3)$$

Furthermore, another constraint is added to ensure a high stability of the MG, which is presented as:

$$T_r(\mathbf{X}) \leq 4 \quad (\text{Nm}) \quad (4)$$

where $T_r(\mathbf{X})$ is the average torque ripple of the inner rotor and outer rotor. This value is designed as 2% of the common torque density of RMCSM-MG [24]. In this study, the torque and torque ripple values were measured using the finite element method (FEM) [27]. The 2D FEM solver adopted in this study is Ansys Maxwell 16.0.

This section is divided into subheadings as follows.

3.1. Taguchi Orthogonal Array Analysis of Objective Function

In the Taguchi sensitivity analysis, each parameter is designed with three levels as shown in Table 2 [23]. The L27 Taguchi Orthogonal Array (TOA) is applied in the analysis. A total of 27 experiments are involved in L27 TOA, and each experiment examines the parameters in a specific combination of levels. Level combinations, experimental results, and the resultant cost values are listed in Table 3. It is worth noting that L1, L2, and L3 are the abbreviations of level 1, level 2, and level 3, respectively.

Then we need to evaluate the average effect of the parameters. This index is the average of the experimental results for one parameter at a certain level. For example, the average effect of X1 at L1 is calculated using the following equation:

$$m_{X1,L1} = \frac{1}{9} \sum_{n=1}^9 C(n) \quad (5)$$

where $C(n)$ represents the results of the n th experiment. Using the same method, we obtained the results shown in Table 4.

Suppose the array element [X1, L1] represents the value in column X1 and row L1. The value represents how much the value of L1 of parameter X1 may influence the cost value. The larger the value, the greater the effect. Therefore, we can extract the most influential level for each parameter. The results illustrate that the parameter combination [L1, L1, L1, L3, L3, L2, L3, L3, L1, L2] is the near-optimal solution. Then, an improved value range is obtained around the near-optimal solution, as shown in Table 5. Considering the actual situation in manufacturing, the lower boundaries of h_{mi} , h_f and h_{mo} are set to 4 mm.

Table 2. Parameter level design.

	X1 (h_{mi})	X2 (h_f)	X3 (h_{mo})	X4 (h_r)	X5 (α_{i1})
Level 1	4 mm	4 mm	4 mm	4 mm	18°
Level 2	8 mm	8 mm	8 mm	8 mm	24°
Level 3	12 mm	12 mm	12 mm	12 mm	36°
	X1 (h_{mi})	X2 (h_f)	X3 (h_{mo})	X4 (h_r)	X5 (α_{i1})
Level 1	18°	60°/17	60°/17	60°/22	60°/22
Level 2	24°	120°/17	120°/17	120°/22	120°/22
Level 3	36°	180°/17	180°/17	180°/22	180°/22

Table 3. L27 Taguchi orthogonal array and experimental results for objective function.

No.	X1	X2	X3	X4	X5	X6	X7	X8	X9	X10	C(X)
1	L1	47.39									
2	L1	L1	L1	L1	L2	L2	L2	L2	L2	L2	69.29
3	L1	L1	L1	L1	L3	L3	L3	L3	L3	L3	112.18
4	L1	L2	L2	L2	L1	L1	L1	L2	L2	L2	37.28
5	L1	L2	L2	L2	L2	L2	L2	L3	L3	L3	60.19
6	L1	L2	L2	L2	L3	L3	L3	L1	L1	L1	80.14
7	L1	L3	L3	L3	L1	L1	L1	L3	L3	L3	29.13
8	L1	L3	L3	L3	L2	L2	L2	L1	L1	L1	45.86
9	L1	L3	L3	L3	L3	L3	L3	L2	L2	L2	83.24
10	L2	L1	L2	L3	L1	L2	L3	L1	L2	L3	112.43
11	L2	L1	L2	L3	L2	L3	L1	L2	L3	L1	13.08
12	L2	L1	L2	L3	L3	L1	L2	L3	L1	L2	71.91
13	L2	L2	L3	L1	L1	L2	L3	L2	L3	L1	39.62
14	L2	L2	L3	L1	L2	L3	L1	L3	L1	L2	56.42
15	L2	L2	L3	L1	L3	L1	L2	L1	L2	L3	61.95
16	L2	L3	L1	L2	L1	L2	L3	L3	L1	L2	108.48
17	L2	L3	L1	L2	L2	L3	L1	L1	L2	L3	27.85
18	L2	L3	L1	L2	L3	L1	L2	L2	L3	L1	44.07
19	L3	L1	L3	L2	L1	L3	L2	L1	L3	L2	51.76
20	L3	L1	L3	L2	L2	L1	L3	L2	L1	L3	53.78
21	L3	L1	L3	L2	L3	L2	L1	L3	L2	L1	23.84
22	L3	L2	L1	L3	L1	L3	L2	L2	L1	L3	82.40
23	L3	L2	L1	L3	L2	L1	L3	L3	L2	L1	68.20
24	L3	L2	L1	L3	L3	L2	L1	L1	L3	L2	35.61
25	L3	L3	L2	L1	L1	L3	L2	L3	L2	L1	32.28
26	L3	L3	L2	L1	L2	L1	L3	L1	L3	L2	83.49
27	L3	L3	L2	L1	L3	L2	L1	L2	L1	L3	35.15

Table 4. Average analysis results.

	X1	X2	X3	X4	X5	X6	X7	X8	X9	X10
L1	62.74	61.74	66.16	59.75	60.08	50.90	33.97	60.71	64.61	43.83
L2	59.53	57.97	58.43	51.62	53.12	58.93	57.74	50.87	57.37	66.38
L3	51.83	54.39	49.51	60.20	60.89	51.94	82.39	62.51	52.12	63.89

Table 5. Original and improved parameter value range.

Parameter	Original Value Range	Improved Value Range
X1(h_{mi})	[4 mm, 20 mm]	[4 mm, 8 mm]
X2(h_f)	[4 mm, 20 mm]	[4 mm, 8 mm]
X3(h_{mo})	[4 mm, 20 mm]	[4 mm, 8 mm]
X4(h_r)	[4 mm, 20 mm]	[8 mm, 16 mm]
X5(α_{i1})	[0°, 36°]	[30°, 42°]
X6(α_{i2})	[0°, 36°]	[24°, 36°]
X7(α_{o1})	[0°, 18°]	[120°/17, 240°/17]
X8(α_{o2})	[0°, 18°]	[120°/17, 240°/17]
X9(α_{m1})	[0°, 18°]	[0°/22, 120°/22]
X10(α_{m2})	[0°, 18°]	[60°/22, 180°/22]

3.2. Sensitivity Analysis and Linear Interpolation Fitting of Torque Ripple Function

To deal with the requirements of the constraint function (4), initially, a study of the sensitivity of each parameter to the constraint function $T_r(\mathbf{X})$ was conducted. Moreover, the most influential parameters were selected to perform the linear interpolation fitting of $T_r(\mathbf{X})$ [28]. Therefore, the value that fulfills the fitting can be considered to be approximately satisfied with the constraint function.

In this study, the parameters are further divided into three levels within the improved value ranges in Table 5. The new level design is shown in Table 6. Then, the L27 TOA, using the parameter level design shown in Table 7, was conducted to obtain the results for $T_r(\mathbf{X})$. Subsequently, the analysis of variance (ANOVA) technique was employed to obtain the influence of each parameter [14]. For instance, the sum of the square of the parameter X1 SS_{X1} is governed by the formula:

$$SS_{X1} = (tm_{X1,L1} - tm)^2 + (tm_{X1,L2} - tm)^2 + (tm_{X1,L3} - tm)^2 \quad (6)$$

where tm represents the total average $T_r(\mathbf{X})$ value of all experiments. The values $tm_{X1,L1}$, $tm_{X1,L2}$, and $tm_{X1,L3}$ represent the average $T_r(\mathbf{X})$ values of parameter X1 in level 1, level 2, and level 3, respectively. The ANOVA results are shown in Table 7. The SS value represents the degree of sensitivity. The larger the value, the more obvious the influence of this parameter on torque ripple. Table 7 also includes the percentage of influence of each parameter. It can be seen that the parameters X5, X6, X7, and X8 are the four most effective factors on $T_r(\mathbf{X})$. In order to reduce the level of computation, all parameters except for X5, X6, X7, and X8 were ignored in the linear interpolation fitting.

Table 6. Parameter level design of torque ripple function.

	X1 (hmi)	X2 (hf)	X3 (hmo)	X4 (hr)	X5 (α_{i1})
Level 1	4 mm	4 mm	4 mm	8 mm	30°
Level 2	6 mm	6 mm	6 mm	12 mm	36°
Level 3	8 mm	8 mm	8 mm	16 mm	42°
	X6 (α_{i2})	X7 (α_{o1})	X8 (α_{o2})	X9 (α_{m1})	X10 (α_{m2})
Level 1	24°	120°/17	120°/17	0°/22	60°/22
Level 2	30°	180°/17	180°/17	60°/22	120°/22
Level 3	36°	240°/17	240°/17	120°/22	180°/22

Table 7. Average analysis results.

	X1	X2	X3	X4	X5	X6	X7	X8	X9	X10
SS	0.04	0.11	0.25	0.03	1.77	1.87	1.74	1.68	0.68	0.81
PC(%)	0.44	1.22	2.78	0.33	19.7	20.8	19.4	18.7	7.57	9.02

The α_{i1} and α_{i2} for the inner layer and the α_{o1} and α_{o2} for the outer layer were discussed during fitting. In the sampling process, 20 groups of experimental results of the average torque ripple versus $(\alpha_{i1}, \alpha_{i2})$ and $(\alpha_{o1}, \alpha_{o2})$ were obtained. All the parameter values are randomly generated from the improved value range. After the linear interpolation fitting, the curve of the average torque ripple versus $(\alpha_{i1}, \alpha_{i2})$ and $(\alpha_{o1}, \alpha_{o2})$ can be achieved, the results of which are shown in Figures 5 and 6. The results in Figure 5 show that the torque ripple fulfils the constraint in all $(\alpha_{i1}, \alpha_{i2})$ evaluations. It is worth noting that, by introducing the interpolation fitting, the torque ripple may become negative, which is unnatural. Therefore, these values are modified to zero in this study. From the data in Figure 6, a polynomial fitting can be achieved to satisfy the constraint function in (4). The polynomial fitting result is as follows:

$$\alpha_{o2} + 0.001\alpha_{o1}^3 - 0.056\alpha_{o1}^2 + 1.625\alpha_{o1} - 21.73 > 0 \quad (7)$$

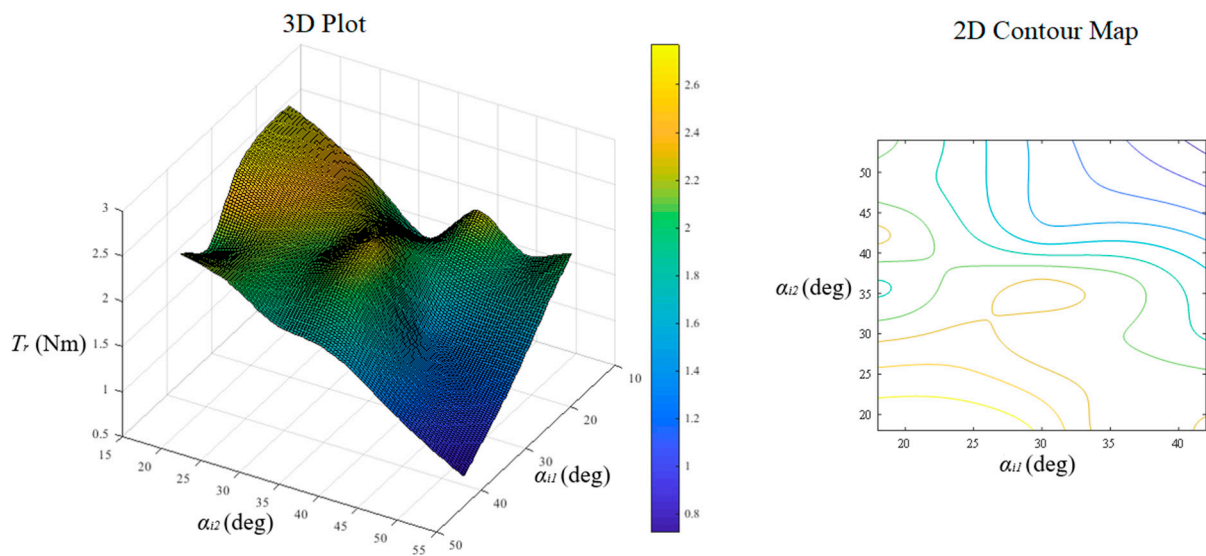


Figure 5. Torque ripple versus α_{i1} and α_{i2} .

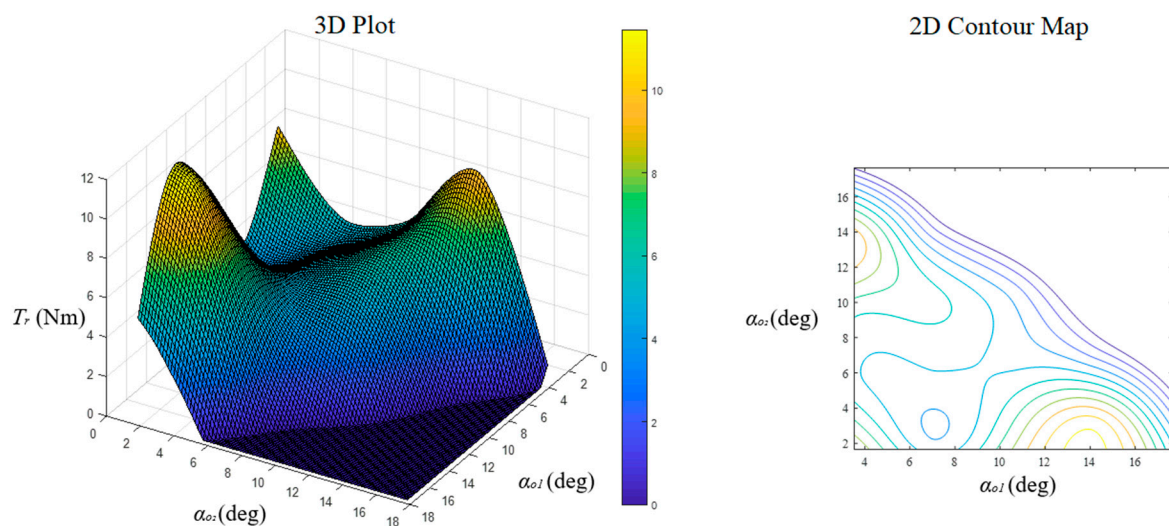


Figure 6. Torque ripple versus α_{o1} and α_{o2} .

3.3. Establishing Optimization

The last step was to establish optimization by combining the sensitivity analysis results. In this study, we used the GA optimization method refined by the improved value ranges and constraint functions.

The crossover probability was set as 0.7 and the mutation probability was set as 0.15 [29]. The maximum optimization generation G_{\max} was set as 40, where each generation contained 60 individuals. The convergence condition is as follows:

$$\begin{aligned} |C^i(\mathbf{x}) - C^{i-1}(\mathbf{x})| &\leq 0.1 \\ i &= 1, 2, \dots, G_{\max} \end{aligned} \quad (8)$$

where $C^i(\mathbf{x})$ represents the best solution of the objective function in the i th generation. The optimization is supposed to finish when it attains the convergence condition or reaches the maximum generation.

3.4. Optimization Results Discussions

Without a sensitivity analysis, optimization is performed within a given original value range which may be very costly in terms of time and computational resources. Indeed,

the optimization results always fall into local optimality when using the original value range. Therefore, the study of a sensitivity analysis based on the Taguchi method, and the linear interpolation fitting of the torque ripple constraint, is essential. According to the analysis results, the GA optimization is refined with a more precise value range (Table 5) and constraint function (7).

Figure 7 shows the cost value variation in each generation of the refined optimization process. The optimization converges after 11 generations. The configuration and torque performance of both the optimized model and original model are shown in Figures 8 and 9, respectively. The average torque of the inner rotor and outer rotor increases by about 47% after optimization. However, the torque ripple increases by about 17% after optimization but still satisfies the constraint in (4). The average torque per unit PM volume before and after optimization is about 163.72 kNm/m^3 and 225.41 kNm/m^3 , respectively. The average torque per unit PM volume increases by about 38%.

Detailed optimized parameter values are shown in Table 8.

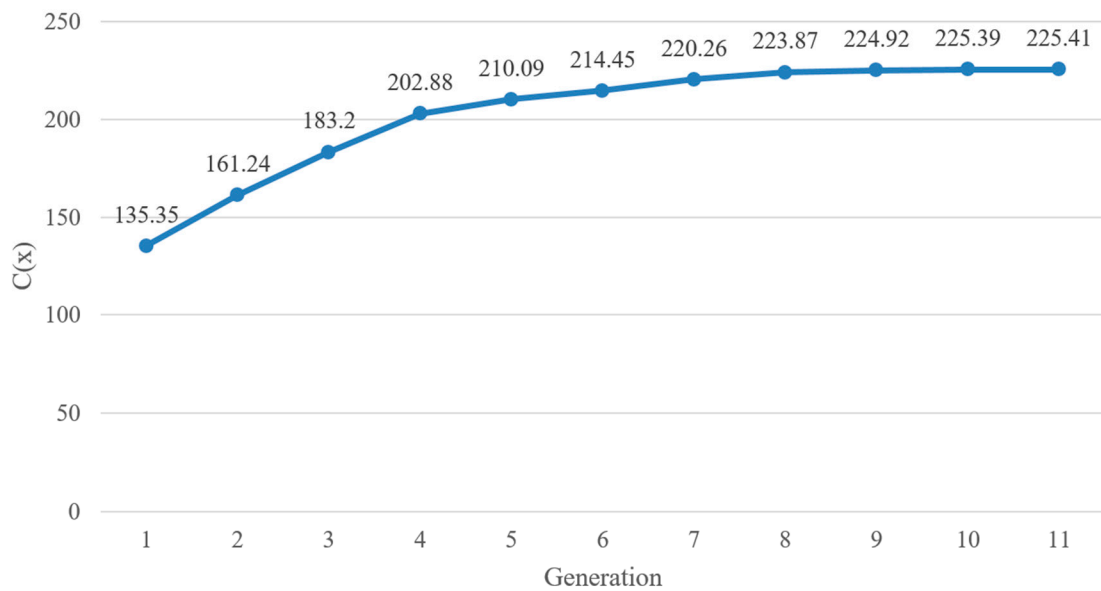


Figure 7. Cost value variation in each generation.

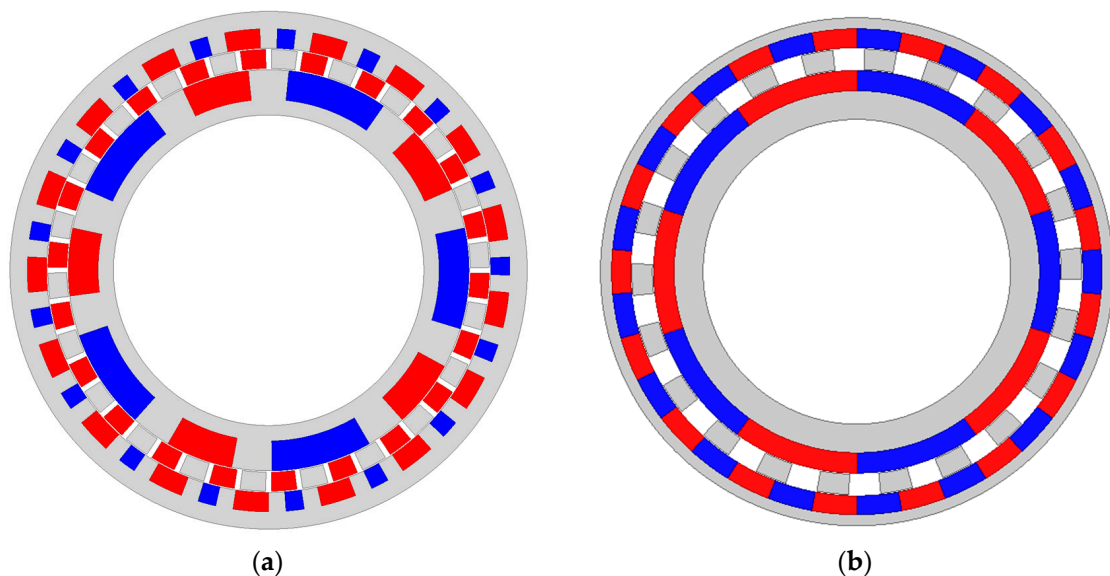


Figure 8. (a) Configuration of the original model. (b) Configuration of the optimized model.

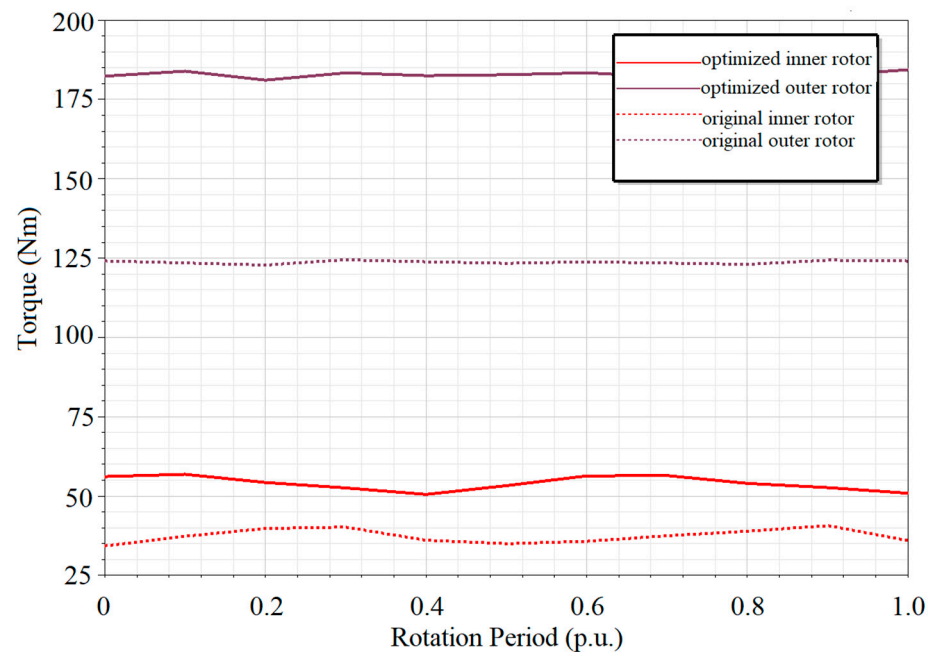


Figure 9. Torque performance of the optimized and original model.

Table 8. Parameters of the original model and optimized model.

Parameter	Original Model	Optimized Model
X1 (h_{mi})	11.54 mm	7.9 mm
X2 (h_f)	7.31 mm	8.0 mm
X3 (h_{mo})	7.49 mm	7.4 mm
X4 (h_r)	5.95 mm	11.3 mm
X5 (α_{i1})	19.5 deg	35.8 deg
X6 (α_{i2})	28.8 deg	36.1 deg
X7 (α_{o1})	8.5 deg	10.4 deg
X8 (α_{o2})	4.3 deg	10.6 deg
X9 (α_{m1})	6.6 deg	0.0 deg
X10 (α_{m2})	6.7 deg	8.2 deg

4. Conclusions

The present study makes several noteworthy contributions towards optimizing a general topology pattern for RMCSM-MG. This pattern can cover most of the common types of MGs. The objective is to discover the MG topology with the highest torque per PM volume. Moreover, the torque ripple should be kept within a reasonable range. To discover the optimal topology, the GA optimization method was conducted. In order to reduce the possibility of local convergence and increase the computational cost, the parameter value range was refined using a sensitivity analysis based on the Taguchi method and interpolation fitting. The optimization converges after 11 generations. After optimization, the average torque increases by about 47%, and the average torque per PM volume increases by about 38%.

Author Contributions: Conceptualization, Y.M. and Y.Y.; methodology, Y.M.; software, Y.M.; validation, Y.M. and Y.Y.; formal analysis, Y.M.; investigation, Y.M.; resources, Y.Y.; data curation, Y.M.; writing—original draft preparation, Y.M.; writing—review and editing, Y.Y.; funding acquisition, Y.Y. All authors have read and agreed to the published version of the manuscript.

Funding: This research was funded by Guangdong Basic and Applied Basic Research Foundation 2022A1515010708 and Start-up Fund of PolyU P0036194.

Institutional Review Board Statement: Not applicable.

Informed Consent Statement: Not applicable.

Data Availability Statement: Not applicable.

Conflicts of Interest: The authors declare no conflict of interest.

References

1. Polinder, H.; Ferreira, J.A.; Jensen, B.B.; Abrahamsen, A.B.; Atallah, K.; McMahon, R.A. Trends in wind turbine generator systems. *IEEE Trans. Emerg. Sel. Top. Power Electron.* **2013**, *1*, 174–185. [[CrossRef](#)]
2. Rasmussen, P.O.; Andersen, T.O.; Jorgensen, F.T.; Nielsen, O. Development of a high-performance magnetic gear. *IEEE Trans. Ind. Appl.* **2005**, *41*, 764–770. [[CrossRef](#)]
3. Peng, S.; Fu, W.N.; Ho, S.L. A novel high torque-density triple permanent-magnet-excited magnetic gear. *IEEE Trans. Magn.* **2014**, *50*, 6971416. [[CrossRef](#)]
4. Atallah, K.; Calverley, S.D.; Howe, D. Design analysis and realisation of a high-performance magnetic gear. *IEEE Proc. Elect. Power Appl.* **2004**, *151*, 135–143. [[CrossRef](#)]
5. Gouda, E.; Mezani, S.; Baghli, L.; Rezzoug, A. Comparative study between mechanical and magnetic planetary gears. *IEEE Trans. Magn.* **2011**, *47*, 439–450. [[CrossRef](#)]
6. Niu, S.; Mao, Y. A Comparative Study of Novel Topologies of Magnetic Gears. *Energies* **2016**, *9*, 773. [[CrossRef](#)]
7. Chen, Y.; Fu, W.N.; Ho, S.L.; Liu, H. A quantitative comparison analysis of radial-flux transverse-flux and axial-flux magnetic gears. *IEEE Trans. Magn.* **2014**, *50*, 8104604. [[CrossRef](#)]
8. Ho, S.L.; Yang, S.Y.; Ni, G.Z.; Wong, H.C. A particle swarm optimization method with enhanced global search ability for design optimizations of electromagnetic devices. *IEEE Trans. Magn.* **2006**, *42*, 1107–1110. [[CrossRef](#)]
9. Zhao, X.; Niu, S. Design and Optimization of a New Magnetic-Geared Pole-Changing Hybrid Excitation Machine. *IEEE Trans. Ind. Electron.* **2017**, *64*, 9943–9952. [[CrossRef](#)]
10. Ho, S.L.; Niu, S.; Fu, W.N. A new dual-stator bidirectional-modulated PM machine and its optimization. *IEEE Trans. Magn.* **2014**, *50*, 8103404. [[CrossRef](#)]
11. Niu, S.; Chen, N.; Ho, S.L.; Fu, W.N. Design optimization of magnetic gears using mesh adjustable finite-element algorithm for improved torque. *IEEE Trans. Magn.* **2012**, *48*, 4156–4159. [[CrossRef](#)]
12. Preis, K.; Magele, C.; Biro, O. FEM and evolution strategies in the optimal-design of electromagnetic devices. *IEEE Trans. Magn.* **1990**, *26*, 2181–2183. [[CrossRef](#)]
13. Dang, D.C.; Friedrich, T.; Kötzing, T.; Krejca, M.S.; Lehre, P.K.; Oliveto, P.S.; Sudholt, D.; Sutton, A.M. Escaping Local Optima Using Crossover With Emergent Diversity. *IEEE Trans. Evol. Comput.* **2018**, *22*, 484–497. [[CrossRef](#)]
14. Hasani, H.M. Design optimization of PID controller in automatic voltage regulator system using Taguchi combined genetic algorithm method. *IEEE Syst. J.* **2013**, *7*, 825–831. [[CrossRef](#)]
15. Wang, H.T.; Liu, Z.J. Application of Taguchi method to robust design of BLDC motor performance. *IEEE Trans. Magn.* **1999**, *35*, 3700–3702. [[CrossRef](#)]
16. Hwang, C.C.; Chang, C.M.; Liu, C.T. A Fuzzy-Based Taguchi Method for Multiobjective Design of PM Motors. *IEEE Trans. Magn.* **2013**, *49*, 2153–2156. [[CrossRef](#)]
17. Zaman, M.A.; Matin, M.A. Optimization of Jiles-Atherton Hysteresis Model Parameters Using Taguchi’s Method. *IEEE Trans. Magn.* **2014**, *51*, 7301004. [[CrossRef](#)]
18. Weng, W.C.; Yang, F.; Elsherbili, A.Z. Linear Antenna Array Synthesis Using Taguchi’s Method: A Novel Optimization Technique in Electromagnetics. *IEEE Trans. Antennas Propag.* **2007**, *55*, 723–730. [[CrossRef](#)]
19. Zaman, M.A. Photonic radiative cooler optimization using Taguchi’s method. *Int. J. Therm. Sci.* **2019**, *144*, 21–26. [[CrossRef](#)]
20. Chou, P.Y.; Tsai, J.T.; Chou, J.H. Modeling and Optimizing Tensile Strength and Yield Point on a Steel Bar Using an Artificial Neural Network with Taguchi Particle Swarm Optimizer. *IEEE Access* **2016**, *4*, 585–593. [[CrossRef](#)]
21. Tsai, J.T.; Liu, T.K.; Chou, J.H. Hybrid Taguchi-genetic algorithm for global numerical optimization. *IEEE Trans. EComput.* **2004**, *8*, 365–377. [[CrossRef](#)]
22. Warren, C.; Giannopoulos, A. Creating finite-difference time-domain models of commercial ground-penetrating radar antennas using Taguchi’s optimization method. *Geophysics* **2011**, *76*, G37–G47. [[CrossRef](#)]
23. Mao, Y.; Niu, S.X. Sensitivity Analysis Based Optimization of General Magnetic Gear Patterns. In Proceedings of the Compumag 2019, Paris, France, 15–19 July 2019.
24. Atallah, K.; Howe, D. A novel high-performance magnetic gear. *IEEE Trans. Magn.* **2001**, *37*, 2844–2846. [[CrossRef](#)]
25. Mao, Y.; Niu, S.; Yang, Y. Differential evolution based multi-objective optimization of the electrical continuously variable transmission system. *IEEE Trans. Ind. Electron.* **2018**, *65*, 2080–2089. [[CrossRef](#)]
26. Ashabani, M.; Abdel-Rady, Y.; Mohamed, I.; Milimonfared, J. Optimum design of tubular permanent-magnet motors for thrust characteristics improvement by combined Taguchi-neural network approach. *IEEE Trans. Magn.* **2010**, *46*, 4092–4100. [[CrossRef](#)]

27. Mao, Y.; Niu, S. Topology Exploration and Analysis of a Novel Winding Factor Modulation Based Hybrid-Excited Biased-Flux Machine. *IEEE J. Emerg. Sel. Top. Power Electron.* **2022**, *10*, 1788–1799. [[CrossRef](#)]
28. Jiang, P.; Liu, F.; Wang, J.; Song, Y. Cuckoo search-designated fractal interpolation functions with winner combination for estimating missing values in time series. *Appl. Math. Model.* **2016**, *40*, 9692–9718. [[CrossRef](#)]
29. Yang, Y.; Tan, S.; Hui, S.Y. Front-end parameter monitoring method based on two-layer adaptive differential evolution for SS-compensated wireless power transfer systems. *IEEE Trans. Ind. Inform.* **2019**, *15*, 6101–6113. [[CrossRef](#)]